

Spin Chirality, Berry Phase, and Anomalous Hall Effect in a Frustrated Ferromagnet

Y. Taguchi,¹ Y. Oohara,² H. Yoshizawa,² N. Nagaosa,^{1,3}
Y. Tokura^{1,3}

An electron hopping on non-coplanar spin sites with spin chirality obtains a complex phase factor (Berry phase) in its quantum mechanical amplitude that acts as an internal magnetic field, and is predicted to manifest itself in the Hall effect when it is not cancelled. The present combined work of transport measurement, neutron scattering, and theoretical calculation provides evidence that the gigantic anomalous Hall effect observed in $\text{Nd}_2\text{Mo}_2\text{O}_7$, a pyrochlore ferromagnet with geometrically frustrated lattice structure, is mostly due to the spin chirality and the associated Berry phase originating from the Mo spin tilting.

When an electron hops between atoms in solids under magnetic field \mathbf{B} , the quantum mechanical amplitude obtains a complex factor with its phase determined by the vector potential \mathbf{A} corresponding to \mathbf{B} ($= \nabla \times \mathbf{A}$). In metallic magnets, the analogous complex factor occurs when an electron hops along the non-coplanar spin configurations, and the effective magnetic field is represented by the spin chirality, namely the solid angle subtended by the spins. This internal effective magnetic field is expected to manifest itself in the Hall effect (1, 2)—the voltage drop transverse to the applied current and external magnetic field. The transverse resistivity ρ_H in ferromagnets consists of two contributions: $\rho_H = R_o B + 4\pi R_s M$, where B is magnetic induction, M is the magnetization, R_o is the ordinary Hall coefficient, and R_s is the anomalous Hall coefficient. The second term, which is proportional to the magnetization, is the anomalous Hall effect (AHE). Conventionally, the AHE has been ascribed to spin-orbit interaction and the spin polarization of conduction electrons, which result in asymmetry in terms of orbital angular momentum (3), or to the asymmetric skew scattering of conduction electrons by the fluctuation of localized moments (4). These theories assume the collinear spin structure. Recently, however, the relevance of the non-coplanar spin configuration to the AHE has been discussed in the context of perovskite-type manganites at high temperatures (1, 5, 6).

In manganites or related double-exchange ferromagnets, as a result of the strong Hund's-rule coupling between the e_g conduc-

tion electrons and the localized t_{2g} spins, the transfer integral from site i to site j is given by $t_{ij} = t\{\cos(\theta_i/2)\cos(\theta_j/2) + \sin(\theta_i/2)\sin(\theta_j/2)\exp[i(\phi_i - \phi_j)]\}$ (7), where θ_i and ϕ_i are the polar coordinates of the spin direction. This transfer integral is a complex number and could produce the gauge flux (8, 9). When we consider an electron hopping along a loop $1 \rightarrow 2 \rightarrow 3 \rightarrow 1$, the total phase acquired by the electron is the solid angle

subtended by the three spins (Fig. 1A) and is proportional to the spin chirality $\mathbf{S}_1 \cdot \mathbf{S}_2 \times \mathbf{S}_3$. Such a gauge flux acts as a fictitious magnetic field \mathbf{b} and affects the charge dynamics in the same way as a real magnetic field does. At finite temperatures, the spin configuration is disordered by thermal agitation, and the topological excitations (called skyrmions) are activated to produce a finite spin chirality that contributes to the transverse conductivity (I). However, it is rather difficult to specify uniquely the mechanism of AHE at finite temperature: The anomalous Hall term vanishes at low temperatures in the manganites, much as it does in conventional ferromagnets (10), and the temperature dependence may not be contradictory, at least qualitatively, to the existing theories (3, 4). At zero temperature, the periodicity of the crystal causes the uniform component of the gauge flux to vanish. As discussed recently (2), the geometrical and topological properties of the lattice are crucial for the Berry phase mechanism of AHE at $T = 0$ K, and Kagome and pyrochlore lattice are two of the rare structures that satisfy this condition. In the ground state of a ferromagnet, there is no thermal or quantum fluctuation. Therefore, the connection between spin configuration and transport properties can be studied in an unambiguous way. Here, we present an anomalous experimental

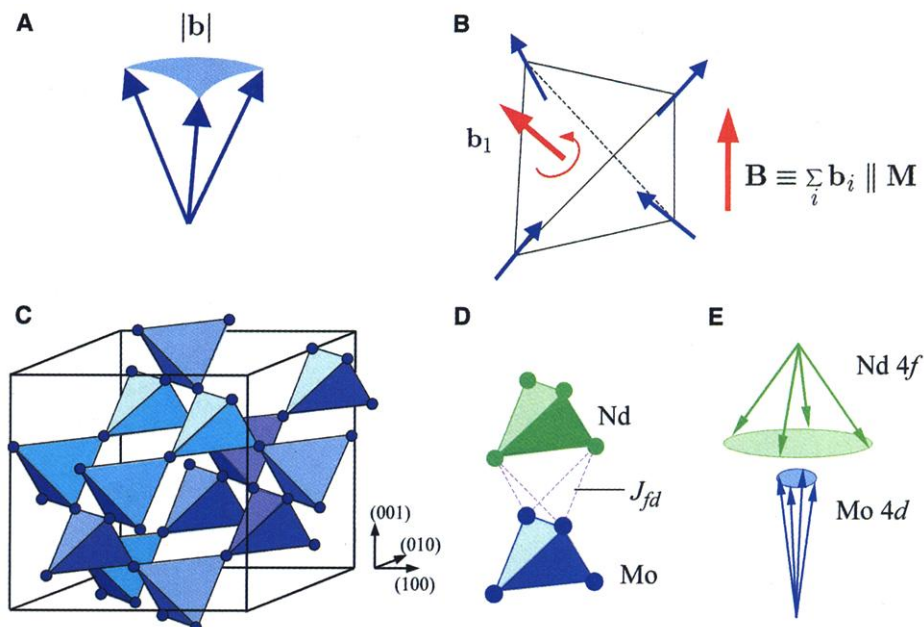


Fig. 1. Schematic magnetic and crystal structures of pyrochlore. (A) Spin chirality, that is, the solid angle subtended by the three spins. (B) "Two-in, two-out" spin structure, in which each spin points along the line that connects the center of the tetrahedron and the vertex. The total fictitious magnetic field is the vector sum of each fictitious magnetic flux that penetrates each plaquette. (C) The B sublattice of pyrochlore structure $\text{A}_2\text{B}_2\text{O}_7$. The A sublattice is structurally identical with this one, but is displaced by half a lattice constant. (D) Relative position of Nd tetrahedron (green circles) and Mo tetrahedron (blue circles) in $\text{Nd}_2\text{Mo}_2\text{O}_7$ pyrochlore. (E) The "umbrella" structure observed for $\text{Nd}_2\text{Mo}_2\text{O}_7$ ($\text{A} = \text{Nd}$, $\text{B} = \text{Mo}$) by a neutron diffraction study. Magnetic unit cell contains four inequivalent Nd $4f$ moments \mathbf{n}_i and four Mo $4d$ moments \mathbf{m}_i . In the umbrella structure, $(\mathbf{m}_i - \mathbf{m}) \perp \mathbf{m}$ and $(\mathbf{n}_i - \mathbf{n}) \perp \mathbf{n}$ for each \mathbf{m}_i and \mathbf{n}_i , where \mathbf{m} and \mathbf{n} are the average moments of four \mathbf{m}_i and four \mathbf{n}_i , respectively.

¹Department of Applied Physics, University of Tokyo, Tokyo 113-8656, Japan. ²Neutron Scattering Laboratory, Institute for Solid State Physics, University of Tokyo, Tokyo, Ibaraki 319-1106, Japan. ³Correlated Electron Research Center (CERC) and Joint Research Center for Atom Technology (JRCAT), Tsukuba 305-0046, Japan.

observation that the AHE continuously increases down to the ground state in a ferromagnet, $\text{Nd}_2\text{Mo}_2\text{O}_7$, with a pyrochlore lattice. This behavior is distinct from the prediction of the existing theories (3, 4) and from experimental results for a broad range of ferromagnetic materials (5, 10, 11), but is in accord with the prediction of Berry phase theory (2).

The pyrochlore-type structure ($\text{A}_2\text{B}_2\text{O}_7$) is well known as a geometrically frustrated lattice (12) and is composed of two sublattices of A and B sites. These sublattices are structurally identical but are displaced by half a lattice constant from each other. In each sublattice, the ions form an infinite network of corner-sharing tetrahedra (Fig. 1C). This connectivity between the magnetic sites gives rise to magnetic frustration, which may lead to intriguing spin states such as spin glass (13). On the other hand, the rare-earth 4f moments are subject to strong spin anisotropy with the easy axis pointing to the center of each tetrahedron. One of the sixfold degenerate “two-in, two-out” spin states in the “spin-ice” model is depicted in Fig. 1B (14). This degeneracy prevents ferromagnetic ordering at finite temperature (14, 15). Another important feature of the spin-ice state is that the total gauge flux for the tetrahedron, which is a vector sum of the flux that penetrates each triangle, is finite and parallel to the total magnetization \mathbf{M} .

In $\text{R}_2\text{Mo}_2\text{O}_7$ materials (where R is a rare-

earth ion), the ground state changes from a spin-glass insulator to a ferromagnetic metal with the change of R (16, 17). $\text{Nd}_2\text{Mo}_2\text{O}_7$ (R = Nd) shows the ground state of a ferromagnetic metal (16), in which the Mo spin-polarized *d* electrons are itinerant while the Nd *f* electrons are viewed as localized and forming the local moments. The Curie temperature is ~ 90 K and the saturated Mo spin moment at low temperature is $\sim 1.5 \mu_B$ (where μ_B is the Bohr magneton). The easy axis of the magnetization is along the (100) direction. Figure 1D shows the relative position of a Nd tetrahedron and a Mo tetrahedron, where another tetrahedron is formed by two Nd ions and two Mo ions. Therefore, the spin chirality of Nd moments is transmitted to the Mo spins via the *f-d* exchange interaction J_{fd} and a conduction electron moving in the Mo sublattice would feel a fictitious magnetic field that is parallel to \mathbf{M} .

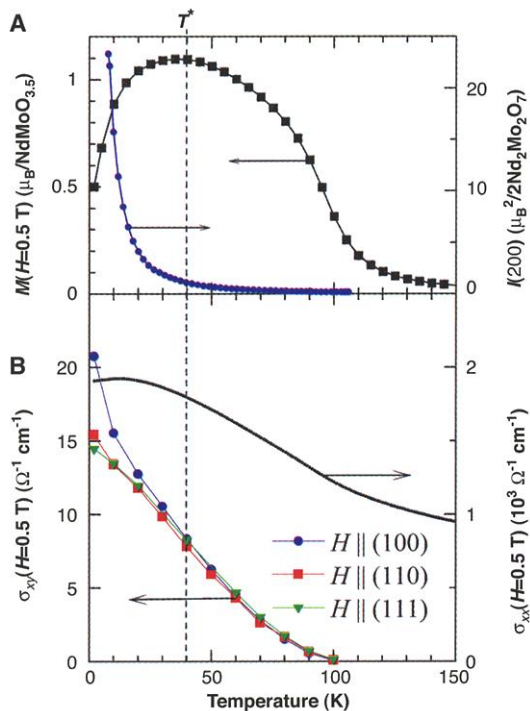
We plot the temperature variation of magnetization and longitudinal conductivity $\sigma_{xx} \approx 1/\rho_{xx}$, both measured at a field of $H = 0.5$ T, in Fig. 2. The magnetization increases rapidly below Curie temperature $T_C = 89$ K, which corresponds to the ferromagnetic ordering of Mo spins. The Nd moments are then subject to the effective magnetic field through the antiferromagnetic J_{fd} , and one of the sixfold degenerate two-in, two-out spin states has more weight than the others. At a crossover temperature ≈ 40 K (which we designate T^* hereafter),

the magnetization begins to decrease while the neutron scattering intensity of the (200) reflection begins to grow (Fig. 2A). We have determined the magnetic structure from the neutron scattering data of (111) and (200) reflections as well as the low-field magnetization data (Fig. 2A) in the following manner (18): The magnetic unit cell contains four inequivalent Nd 4f moments \mathbf{n}_i and four Mo 4d moments \mathbf{m}_i . From a general energetic argument that takes into account the nearest-neighbor exchange interaction, we can infer that the “umbrella structure” (Fig. 1E) is stable. This reduces the number of unknown parameters to four, namely, the magnitudes and tilting angles of the Nd and Mo moments. The scattering intensities I_1 , I_2 , and I_3 corresponding to the (111), (200), and (000) reflections, which are normalized in a unit of μ_B^2 per magnetic unit cell, can be expressed in terms of the four parameters. In the actual procedure, I_3 data were replaced by the uniform magnetization data with high accuracy, and the magnitude of the Mo moment below T^* was extrapolated from the values at higher temperatures. Thus, we could determine three unknown parameters from three experimental constraints. It turns out that the Nd moments grow rapidly below T^* , with their total moment pointing antiparallel to the total Mo spin. The tilting angles of the Nd and Mo moments (θ_n and θ_m , respectively) are estimated to be $\theta_n \approx 70^\circ$ to 80° and $|\theta_m| < 10^\circ$ at 8 K (see below).

Figure 3A shows the magnetic field dependence of magnetization of a single crystal of $\text{Nd}_2\text{Mo}_2\text{O}_7$ at several temperatures when the magnetic field is applied along the (100) direction. The magnetization monotonically increases with decreasing temperature to $T^* \approx 40$ K at both low and high fields. Below T^* , in contrast, the magnetization at a low field (e.g., 0.5 T) decreases, reflecting the rapid growth of Nd moments with their total moment pointing antiparallel to that of the Mo spin. However, the Nd moment is very susceptible to the magnetic field at low temperatures (for free Nd^{3+} ion at $H = 10$ T and $T = 2$ K, $g_J \mu_B H/k_B T = 11$, where g_J is the Landé *g* factor and k_B is the Boltzmann constant). Therefore, the total magnetization shows a substantial increase with application of high magnetic field at 2 K.

In plotting the magnetic field dependence of the Hall resistivity ρ_H at various temperatures (Fig. 3B) with the magnetic field \mathbf{H} also applied along the (100) direction, the anomalous term is dominant over the ordinary term at all the temperatures. Because the ordinary term is negligible at a weak magnetic field, the value of ρ_H at 0.5 T can be a good measure of the anomalous term. This quantity continues to increase down to the lowest

Fig. 2. Temperature evolution of magnetic and transport properties. (A) Temperature dependence of magnetization at $H = 0.5$ T and the background-subtracted and properly normalized neutron scattering intensity I of the (200) reflection, which represents the ordering of the transverse component. (B) Temperature dependence of the longitudinal conductivity σ_{xx} at $H = 0.5$ T and the Hall conductivity σ_{xy} at $H = 0.5$ T. The value of σ_{xy} at $H = 0.5$ T is derived from the values of ρ_H and ρ_{xx} at $H = 0.5$ T through the relation $\sigma_{xy} = \rho_H/(\rho_{xx}^2 + \rho_H^2)$. Single crystals of $\text{Nd}_2\text{Mo}_2\text{O}_7$ were grown by the floating-zone method in Ar atmosphere. Typical size is 4 mm in diameter and 30 mm in length. The Curie temperature of the crystal used for the transport measurements is 89 K. The Hall effect and resistivity measurements were done by the conventional method. Neutron diffraction measurements were carried out on a general-purpose triple-axis spectrometer in the JRR-3M of the Japan Atomic Energy Research Institute, Tokai, Japan. An incident neutron momentum $k_i = 2.559 \text{ \AA}^{-1}$ was selected with a pyrolytic graphite filter. The single-crystal sample was placed in an Al can with helium gas, and it was attached at the cold head of a closed-cycle helium gas refrigerator.



temperature, 2 K (Fig. 3B, inset), in marked contrast to the prediction of the existing theories (3, 4) and to experimental results (5, 10, 11). In a plot of the Hall conductivity σ_{xy} at $H = 0.5$ T, together with the results for cases where a magnetic field is applied along high-symmetric directions (110) and (111) (Fig. 2B), the σ_{xy} value for every direction continues to increase below T_C all the way down to the ground state. This is true even below 20 K $\approx T_C/5$, where σ_{xx} changes very little (Fig. 2B). The magnitude of σ_{xy} is almost isotropic above T^* but shows large anisotropy below T^* , clearly indicating an intimate relation with the spin configuration.

The steep decrease of ρ_H in a high-field region at low temperatures (Fig. 3B) is quite remarkable and should be attributed to the anomalous Hall term. If it were due to the ordinary Hall coefficient R_o , the value of R_o would increase by a factor of 5 as T decreases from 40 K to 2 K, which is obviously incompatible with the minimal change in σ_{xx} (Fig. 2B).

As we have argued above, both the temperature and field dependencies of ρ_H are anomalous within the conventional view of AHE. Furthermore, these features strongly suggest that the relevant variable is the directional degree of freedom, rather than the magnitude, of the spin moment: The direction of the spin can vary with the change of temperature or magnetic field even at temperatures well below T_C , whereas its magnitude cannot.

On the basis of the spin chirality mechanism of the AHE, we have calculated σ_{xy} as a function of the tilting angle of the Mo spins using the tight-binding Hamiltonian for triply degenerate t_{2g} bands. In Fig. 4, the calculated results for σ_{xy} are shown as a function of the tilting angle θ_m in the two-in, two-out spin state under the applied field along the (100) direction. We could reproduce the correct sign ($\sigma_{xy} > 0$) and obtained the relation $\sigma_{xy} \propto \theta_m^2$, as is expected from $|b| \propto \theta_m^2$. The magnitude of σ_{xy} is also consistent with the above experimental results; that is, the observed σ_{xy} can be reproduced with $\theta_m \approx 4^\circ$. The conventional on-site spin-orbit interaction $\lambda \approx 400 \text{ cm}^{-1}$ gives comparable or slightly larger values of σ_{xy} , and the value is rather sensitive to the details of the band structure such as the crystal field splitting. However, this mechanism cannot explain the rapid increase of σ_{xy} accompanied by the tilting, because it gives only a weak dependence on θ_m ($\propto \cos \theta_m$).

We also plotted the calculated σ_{xy} for the two-in, two-out structure for the (111) direction. These values are simply $1/\sqrt{3}$ times the values for the (100) direction, because the "easy axis" of the spin chirality is the (100) direction and only $1/\sqrt{3}$ of the fictitious field can affect σ_{xy} . Indeed, the observed anisotropy at 2 K at a low field, $\sigma_{xy}^{(100)}/\sigma_{xy}^{(111)} \approx 1.6$, nearly coincides with the predicted value ($= \sqrt{3}$) (Fig. 4, inset).

The magnetic field dependence of σ_{xy} at low temperatures (Fig. 4, inset) can also be explained in terms of Berry phase theory as a field suppression of the spin chirality. In a low-field region, the tilting angle of the spins is relatively large, which gives rise to the large spin chirality and hence the large anomalous Hall term. Once a high field is applied and the spins are aligned along the field direction, the spin chirality or the fictitious magnetic field is reduced, resulting in the diminished AHE.

At 40 K, σ_{xy} is almost isotropic, in accord with the absence or minute residue of the long-range ordering of the transverse component. The magnetic field dependence of σ_{xy} at 40 K (Fig. 4, inset) is weaker than at 2 K because the Zeeman energy is small compared with the temperature, and the thermal fluctuation of moments cannot be suppressed by the magnetic field.

We have found anomalous temperature and field dependence of the AHE. Below $T^* \approx 40$

Fig. 3. Magnetic field dependence of magnetization and Hall resistivity. (A) Magnetic field dependence of magnetization at various temperatures. The field is applied along the (100) direction. (B) Magnetic field dependence of the Hall resistivity ρ_H with $H \parallel (100)$ at several temperatures. The inset shows the temperature dependence of ρ_H at 0.5 T, which is a measure of the anomalous Hall term. The ρ_H at a low field (< 0.3 T) is finite at 2 K, whereas it tends to zero above 10 K, in accord with the presence or absence of remnant magnetization at the respective temperatures.

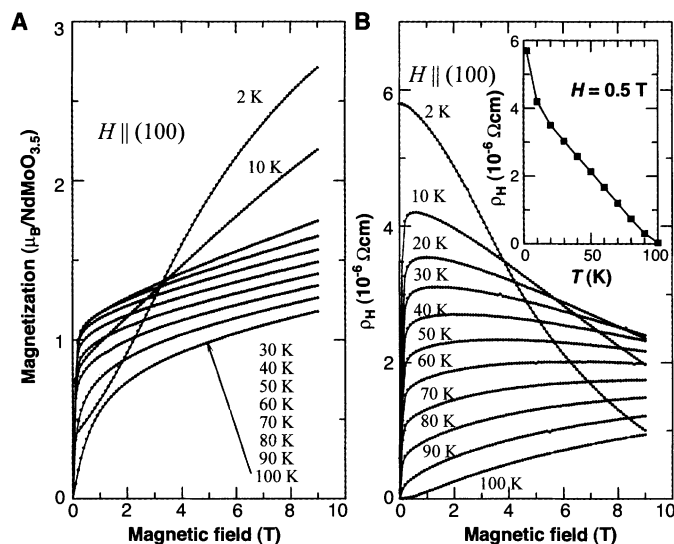
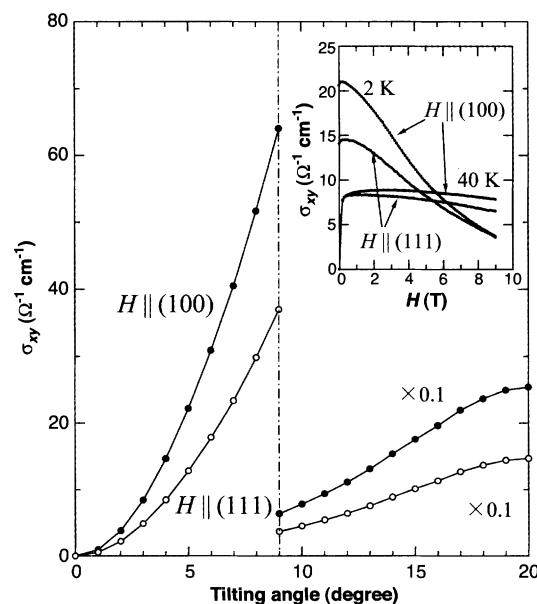


Fig. 4. Theoretical and experimental results of Hall conductivity. The theoretically calculated Hall conductivity σ_{xy} for the two-in, two-out spin configuration for $H \parallel (100)$ (solid circles) is plotted against the tilting angle of the spins. Note the scale change at a tilting angle of 9° . The tight-binding Hamiltonian parameters of $t_{d\sigma} = -0.5$ eV, $t_{d\pi} = 0.1$ eV are used for the triply degenerate t_{2g} bands. The transverse conductivity σ_{xy} is calculated in terms of the Kubo formula, where the k -integral over the first Brillouin zone is replaced by the discrete sum over the $40 \times 40 \times 40$ mesh. The open circles represent $1/\sqrt{3}$ times the respective solid-circle values, which corresponds to the case with $H \parallel (111)$ assuming that the two-in, two-out spin configuration remains stable against the magnetic field. The inset shows the experimental results of σ_{xy} plotted against applied magnetic field. The data below and above T^* are shown for $H \parallel (100)$ and (111) configurations. The experimental zero-field value at 2 K crudely corresponds to the calculated tilting angle of $\sim 4^\circ$ of the Mo spins, which is in accord with the estimate at 8 K as judged by neutron scattering [(18); see also text] and the following molecular-field consideration: Using the moments of Nd and Mo at 50 K derived from the neutron data, we can estimate the molecular field at the Nd site and hence the value of J_{fd} ($= 1.5$ K). Given J_{fd} together with the magnitude and tilting angle of the Nd moments ($\theta_n = 70^\circ$ to 80°) deduced from neutron data at 8 K, the effective transverse field at the Mo site at 8 K produced by the tilted Nd moments can be evaluated. Together with the estimated value of J_{dd} ($= 11$ K), this allows us to estimate the tilting angle of Mo to be 2.4° .



K, where the magnetic structure changes, the Hall conductivity shows clear anisotropy. Such behaviors of the AHE can be successfully ascribed to the Berry phase produced by the spin chirality on the pyrochlore lattice. Our results show that the control of spin texture reflecting lattice topology provides a new way to tailor electronic properties in a variety of magnetic materials in bulk and at interfaces.

References and Notes

1. J. Ye et al., *Phys. Rev. Lett.* **83**, 3737 (1999).
 2. K. Ohgushi, S. Murakami, N. Nagaosa, *Phys. Rev. B* **62**, R6065 (2000).

3. R. Karplus, J. M. Luttinger, *Phys. Rev.* **95**, 1154 (1954).
 4. J. Kondo, *Prog. Theor. Phys. (Kyoto)* **27**, 772 (1962).
 5. P. Matl et al., *Phys. Rev. B* **57**, 10248 (1998).
 6. S. H. Chun, M. B. Salamon, Y. Lyanda-Geller, P. M. Goldbart, P. D. Han, *Phys. Rev. Lett.* **84**, 757 (2000).
 7. P. W. Anderson, H. Hasegawa, *Phys. Rev.* **100**, 675 (1955).
 8. G. Baskaran, P. W. Anderson, *Phys. Rev. B* **37**, 580 (1988).
 9. N. Nagaosa, P. A. Lee, *Phys. Rev. Lett.* **64**, 2450 (1990).
 10. J. P. Jan, J. M. Gijsman, *Physica* **18**, 339 (1952).
 11. R. S. Lee, S. Legvold, *Phys. Rev.* **162**, 431 (1967).
 12. A. P. Ramirez, *Annu. Rev. Mat. Sci.* **24**, 453 (1994).
 13. B. D. Gaulin, J. N. Reimers, T. E. Mason, J. E. Greedan, Z. Tun, *Phys. Rev. Lett.* **69**, 3244 (1991).
 14. M. J. Harris, S. T. Bramwell, D. F. McMorrow, D. F. Zeiske, K. W. Godfrey, *Phys. Rev. Lett.* **79**, 2554 (1997).

15. A. P. Ramirez, A. Hayashi, R. J. Cava, R. Siddharthan, B. S. Shastry, *Nature* **399**, 333 (1999).
 16. N. Ali, M. P. Hill, S. Labroo, J. E. Greedan, *J. Solid State Chem.* **83**, 178 (1989).
 17. T. Katsufuji, H. Y. Hwang, S.-W. Cheong, *Phys. Rev. Lett.* **84**, 1998 (2000).
 18. Y. Oohara, H. Yoshizawa, Y. Taguchi, Y. Tokura, unpublished data.
 19. We thank S. Murakami, K. Ohgushi, and N. Hamada for fruitful discussions. Supported in part by a Grant-in-Aid from the Ministry of Education, Japan, and by the New Energy and Industrial Technology Development Organization.

11 December 2000; accepted 22 February 2001

Alignment of Liquid Crystals with Patterned Isotropic Surfaces

Baek-woon Lee and Noel A. Clark*

The molecules of a nematic liquid crystal exposed to an isotropic surface adopt a mean tilt relative to the normal but have no in-plane alignment—that is, they are free to have any azimuthal orientation in the surface plane. Pursuing the theoretical suggestion by Meyer that, in spite of this azimuthal degeneracy, spatially inhomogeneous isotropic surfaces combine with liquid crystal elastic anisotropy to produce alignment, we show that a boundary line between two isotropic regions that differ in mean tilt does indeed align the liquid crystal. The boundaries on a patterned surface of distinct isotropic regions thus act as a system of lines that the molecular orientation locally follows. This enables the development of liquid crystal alignment surfaces based on printing or lithographic patterning.

Nematic liquid crystals (LCs) are fluids made anisotropic by the spontaneous appearance of long-range molecular orientational order. Their resulting birefringence is large and readily controlled by applied fields and surfaces, rendering nematics useful for electro-optical applications. As a result, a key aspect of any LC device or texture is the nature of the surface interactions and geometry that combine to establish its orientation field. LC alignment surfaces used to date, such as mechanical- or photo-buffed polymer films (1), evaporated oxide (2), crystal surfaces (3), or the more recently developed patterned monolayers (4, 5), all require molecular-level in-plane structural anisotropy (6) or anisotropic surface roughness (7–11) to induce molecular orientation. Control of such treatments comes only by way of trial and error, their effectiveness depending on the details of surface structure and molecular arrangement at the nanometer scale that are difficult to predict. Here we demonstrate that LC alignment can be achieved without molecular-scale anisot-

ropy or roughness, showing that a surface lithographically divided into two distinct molecularly smooth isotropic regions can produce alignment governed only by the pattern of boundary lines between them and by the LC elasticity. This observation opens the way to the application of a variety of powerful lithographic and printing techniques to LC alignment, enabling, for example, spatially varying orientation and anchoring strength determined by surface patterning.

Nematic order is described by the unit vector director $\mathbf{n}(\mathbf{r})$, giving the local average molecular long axis direction. In a nematic exposed to an isotropic surface, $\mathbf{n}(\mathbf{r})$ adopts a mean tilt, θ , relative to the normal, but $\mathbf{n}(\mathbf{r})$ is free to have any azimuthal orientation ϕ about the surface normal (Fig. 1). We use binary isotropic surfaces in which the surface area is divided into two distinct regions of differing θ : The surface is either homeotropic (HO), with \mathbf{n} normal to the surface ($\theta = 0^\circ$), or random planar (RP), with \mathbf{n} parallel to the surface ($\theta = 90^\circ$). A cell with boundaries between such surfaces (magenta lines) is shown in Fig. 2, where the local direction of $\mathbf{n}(\mathbf{r})$ is indicated by the blue sticks. The structure of $\mathbf{n}(\mathbf{r})$ in such a cell is established by the interplay of the enforced surface condition on

θ with the LC elasticity, which resists spatial variation of $\mathbf{n}(\mathbf{r})$. The elemental local deformations of $\mathbf{n}(\mathbf{r})$, bend (B), splay (S), and twist (T), are indicated by the green areas in Fig. 2 and require an elastic energy density $U_X = (1/2)K_X[\partial n_i/\partial s_j]^2$ (where $X = S, B, \text{ or } T$) proportional to the respective Frank elastic constant $K_B, K_S, \text{ or } K_T$ and to the square of the appropriate spatial gradient of $\mathbf{n}(\mathbf{r})$. In general, the elastic constants are not equal, with K_T less than K_B, K_S for known nematics. As a result, in the cell of Fig. 2, the change in orientation imposed at the surface is mediated in the bulk primarily by twist of $\mathbf{n}(\mathbf{r})$, because this is energetically least costly, such that the LC adopts a structure having the mean orientation of \mathbf{n} parallel to the boundary lines. The boundaries of a pattern, then, are a system of lines on the surface which \mathbf{n} locally follows.

Alignment of LCs by spatially inhomogeneous surfaces was proposed by Meyer (12) and Berreman (13) and demonstrated by Ong, Hurd, and Meyer (14), who controlled the mean LC tilt θ by varying the fractional area of $\theta = 0^\circ$ dots in an otherwise planar-aligning ($\theta = 90^\circ$) anisotropic ($\phi = 0^\circ$) obliquely evaporated SiO surface. Also proposed by Meyer (12, 14), and recently analyzed with Landau-deGennes theory (15, 16), is the much more interesting possibility, experimentally realized here, of achieving azimuthal (ϕ) anchoring on isotropic surfaces. Demonstration of these ideas requires elimination of alignment from the molecular interactions and surface topography effects, mentioned above. The surfaces used here were isotropic octadecyltriethoxysilane (OTE) self-assembled monolayers (SAMs) on glass to make the $\theta = 0^\circ$ regions and the surface obtained upon removal of the SAM by exposure to unpolarized, normally incident ultraviolet (UV) light to make the $\theta = 90^\circ$ regions. The frictional and surface relief characteristics of such patterned SAMs were studied extensively by atomic force microscopy (AFM) (17, 18). These data show that both the unexposed SAM and exposed glass areas were isotropic and molecularly smooth. The step in surface relief at the boundaries, on the order of 1 nm high and 100 nm wide, is small enough to

Department of Physics, Ferroelectric Liquid Crystal Materials Research Center, University of Colorado, Boulder, CO 80309-0390, USA.

*To whom correspondence should be addressed.